buildings

MDPI

Article

Multifactorial Chloride Ingress Model for Reinforced Concrete Structures Subjected to Unsaturated Conditions

Enrico Zacchei [1,*] and Emilio Bastidas-Arteaga [2]

[1] Itecons-Institute for Research and Technological Development in Construction, Energy, Environment and Sustainability, Rua Pedro Hispano s/n, 3030-289 Coimbra, Portugal
[2] Laboratory of Engineering Sciences for Environment (LaSIE) UMR CNRS 7356, La Rochelle University, Avenue Michel Crépeau, 17042 La Rochelle, France; ebastida@univ-lr.fr
* Correspondence: enricozacchei@gmail.com

Abstract: The attack of chloride ions is one of the most important factors affecting reinforced concrete (RC) durability. Chloride ingress into concrete is usually studied by assuming constant diffusivity and constant surface chloride concentration. However, these two approximations could badly estimate the chloride concentration in RC structures and then the lifetime assessment. Several factors influence the chloride concentration and ingress mechanisms in the convection area. In this paper, a new multifactorial and multiphase model to account for some effects on chloride surface concentrations in the convection zone is proposed. 136 values have been collected to identify the position and the chloride concentration in the border between the diffusion and convection zones. In addition, a time-dependent multifactorial diffusivity is considered. Diffusivity, which is the key parameter of the mechanical diffusion accounts in this paper for the water/cement ratio, chloride binding, temperature, concrete age, internal humidity, concrete deformation, and damage. The surface chloride model considers environment humidity, temperature, superficial concrete irregularities, and convection area of concrete. Advanced numerical solutions have been carried out to consider space and time dependencies in the model. Results show that the error function-based solutions could underestimate the chloride concentration C for periods < 10 years and for concrete depths > 4.0 cm in comparison with the proposed model.

Keywords: chloride diffusion; superficial chloride; non-constant diffusivity; convection area; concrete irregularities

Citation: Zacchei, E.; Bastidas-Arteaga, E. Multifactorial Chloride Ingress Model for Reinforced Concrete Structures Subjected to Unsaturated Conditions. *Buildings* **2022**, *12*, 107. https://doi.org/10.3390/buildings12020107

Academic Editors: Binsheng (Ben) Zhang and Wei (David) Dong

Received: 18 December 2021
Accepted: 20 January 2022
Published: 23 January 2022

1. Introduction

1.1. Background

A relevant mechanism of deterioration for reinforced concrete (RC) structures is the corrosion of steel bars and concrete elements induced by chloride ion diffusion. Structures that are usually subjected to this attack are placed in aggressive environments (i.e., industrial and coastal zones) as shown in the literature [1–3]. For example, in [2,3] it is shown how the chloride concentration in the atmosphere reaches high values on the coast up to 4500 m from the seashore due to the variations of temperature, humidity, and wind during a year. Also, in [4] it is shown that structures placed up to 6500 m from a coastline could be affected by chloride attacks.

The main transport mechanism of chloride ions in concrete is diffusion, which is a complex non-linear time-dependent process that depends on several intrinsic phenomena, such as capillary absorption and permeation [5,6]. The modeling of ion diffusion is also complicated by the heterogeneity of the concrete, which exists at a variety of scales.

The heterogeneity is due to the composition of the ingredients of the hardened cement paste which are, at the scale of millimeters, water, cement clinker, supplementary cementitious materials, and/or aggregates. At the scale of micro-meters, it is possible to identify

capillary pores, un-hydrated cement, crystalline, and gel hydration products, each with its diffusion properties [7].

The diffusivity parameter, that controls the chloride ingress process, is usually used as a constant value, without considering several factors such as the water/cement ratio, binding chloride ions, temperature, concrete aging, concrete deformation [8], exposure to the de-icing salts [9,10], aggregate volume [11,12]. Therefore, considering these aspects a correct estimation of the diffusivity becomes paramount for improving lifetime assessment. In [13] several empirical models, to estimate the chloride diffusivity, are shown, but each diffusivity would seem non-complete.

In alternative research, the diffusivity is also studied in function of the presence of graphene and silica fume in concrete [14] and the function of recycled aggregate concrete with nanoparticles [15].

The need to propose a new model about the surface chloride concentrations is because its calculus is in many cases carried out by adopting several hypotheses that could under- or over-estimate the final chloride concentration in concrete. For this, two main models have been used to provide more reliable results in terms of chloride concentrations: a multifactorial diffusivity and a multiphase surface chloride concentration.

In several research studies [16–18] the chloride ingress is modeled by using a solution of Fick's law based on the error function that considers that the peak value (i.e., high chloride concentration) is located at the surface of the concrete. However, experimental assessments of chloride profiles show that the peak value happens inside the concrete and near the concrete surface area called "convection area", and thus the chloride concentrations at surface concrete are lower than this peak [19]. Therefore, these experimental observations indicate that the boundary conditions that are usually imposed in Fick's laws are not quite representative of the real chloride ingress process for the convection area. In [13] it is shown that the concrete is "saturated below the outer convection zone of the cover in chloride profiles".

The main difference between convection and diffusion areas is that in the first area (convection) the concrete is not supposed to be saturated and therefore several physical mechanisms affect the chloride ingress process. In the diffusion area, it is supposed that chloride ingress is mainly driven by pure chloride diffusion mechanisms.

Authors of this paper prefer to use the nomenclature "convection area" (or "convection zone") and "diffusion area" (or "diffusion zone"), in accordance with [20,21], to divide two areas instead of using "saturated and non-saturated areas".

In [22,23] it is shown that the surface chloride concentration, C_s, increases in function of the concrete age, up to a defined value where it stabilizes. For this reason, C_s is usually considered constant; but, as already mentioned, this could under- or over-estimate the total chloride concentration C as studied in [24].

In [25–27] through the study of real structures, manly bridges, and offshore structures placed on marine environments, it is also shown how the chloride concentration peak is placed at a certain distance from the concrete surface. In these studies, the chloride concentration, as mentioned, increases from the concrete surface and reaches a peak value inside the concrete, where the pure diffusion, which could be modeled by the Fick laws, starts. From these studies, the mean maximum chloride concentration at the convection zone and the convection zone depth are estimated as ~11.0 kg/m^3 and ~1.5 cm, respectively. The depth value depends on the typology of the studied structures and could be very variable. The mean maximum C_s is ~5.50 kg/m^3.

In [28,29] by experimental tests on beams, analog results were obtained, confirming that the maximum chloride concentration is not placed in the concrete surface (at zero depth). In [30] This phenomenon is shown by experimental laboratory tests to rehabilitate a concrete element. From these studies, the mean maximum chloride concentration at the convection zone and the convection zone depth are ~10.0 kg/m^3 and ~1.0 cm, respectively. Here, the mean maximum C_s is ~6.0 kg/m^3.

From these and other studies [21], several values of chloride concentration and convection zone depths have been collected to estimate new reference values. These values have been well explained in this work, indicating the main environmental and exposure conditions.

Therefore, in this paper, a more complete model is proposed for chloride diffusion to account for the influence of the convection area, the irregularity of the concrete surface, and the external temperature and humidity. Also, a multi-factorial relationship for diffusivity has been used. These conditions directly affect the chloride ion diffusion in the concrete. To carry out this model with a non-constant diffusivity, advanced numerical solutions have been implemented.

1.2. Problem Statement

The flux in the x direction of chloride ions J in concrete [20,31] (diffusion zone) is governed by partial differential equations (PDEs) named as the first (Equation (1)) and second (Equation (2)) Fick's laws, respectively [23,32,33]:

$$J = -D\,\nabla C(x) \tag{1}$$

$$\frac{\partial C(x,t)}{\partial t} = \nabla\cdot(D\,\nabla C(x,t)) = \frac{\partial}{\partial x}\left(D\frac{\partial C(x,\ t)}{\partial x}\right) \tag{2}$$

where ∇C is the total chloride concentration gradient and D is the coefficient of diffusion of chlorides (or diffusivity). Equation (2) comes from Equation (1) by considering the general mass balance in time t and x direction under a non-steady state [23].

A closed-form analytical solution of Equation (2) is obtained as Equation (3) by considering: (i) initial conditions, $C(x,\ t = 0) = C_0$, and (ii) Dirichlet's boundary conditions, $C(x = 0,\ t) = C_s$ and $C(x = \infty,\ t) = C_0$ (i.e., semi-infinite medium), where C_0 and C_s are the inner and surface chloride concentrations, respectively [28,34]. Therefore, Equation (3) is:

$$C = C_0 + (C_s - C_0)\left(1 - \mathrm{erf}\frac{x}{2\sqrt{D\,t}}\right) \tag{3}$$

where erf(·) is the Gaussian error (integrated from 0 to $x/\left(2\sqrt{D\,t}\right)$) [35]. Equation (3) has been widely used for lifetime assessment in this form or it has been developed to consider other factors.

This solution neglects the variations of chloride concentration in the convection zone, the effects of environmental exposure, chloride binding, mechanical loadings, etc. To account for these aspects, a complex numerical solution of coupled PDEs should be required [9,35]. Nevertheless, these models are not easy to use in engineering practice because they require larger user expertise and getting several parameters.

This study proposes an alternative chloride ingress model that considers the effects of environmental exposure, chloride binding, mechanical loads, concrete aging, the convection zone, irregularities in the concrete surface, and variations of the surface chloride concentration. In this sense, these aspects, accounting in a unique way, represent the contributions of this work.

The model could be applied to components placed in non-saturated conditions (i.e., atmospheric zones) [20,31]. Therefore, two areas are considered (see Figure 1) in accordance with [20,21]: (i) convection zone where Equation (3) cannot be applied; and (ii) diffusion zone where Equation (3) or other similar solutions are still valid. Accordingly, the proposed methodology encompasses:

1. a multifactorial diffusion model for the diffusion zone detailed in Section 2;
2. a procedure and models for lifetime assessment that provide an equivalent surface chloride concentration (C_s') in the boundary between the convection and diffusion zones that is located at the distance x' from the concrete surface (see Figure 1). These procedures and models are described in Section 3 and illustrated in Section 4.

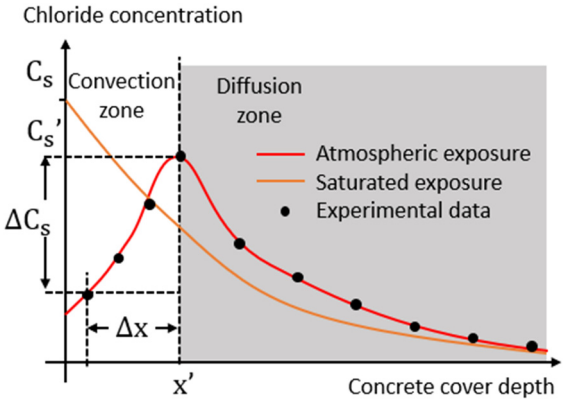

Figure 1. Chloride profiles for atmospheric and saturated exposure conditions.

2. Multifactorial Chloride Ingress Model for Pure Diffusion Zones

2.1. Model Formulation

The chloride ions are mainly transported into a water-saturated or non-saturated (i.e., atmospheric conditions) concrete [20,31] via diffusion. The diffusivity takes place at a very slow rate, e.g., 10^{-13} to 10^{-11} m^2/s [15,17], allowing that the chemical process of multispecies transfer [36] in concrete pores remains in equilibrium during the diffusion at any time (i.e., the chloride binding C_b remains constant). This is because the diffusion happens via water-filled pores and not via air-filled pores [37].

Chloride ingress is also affected by external load conditions, for example, the compaction effect could lead to an increase in chloride diffusion as shown in [38]. This aspect has been accounted for by the f_4 factor, which depends on the elastic deformation ε and damage d (Equation (4)). In this study, the presence of load-induced cracks ($d \neq 0$) has been considered by only adopting experimental values, and thus it should be considered in an indirect way.

The chloride diffusivity D can be considered constant [17], variable [32] or multi-factorial [35]. The multi-factorial relationship considered in this study, recently introduced in [39], is:

$$D = f_0(w/c) \times f_1(C_b) \times f_2(T) \times f_3(t) \times f_4(\varepsilon, d) \times f_5(h) \quad (4)$$

where $f_0(w/c)$, $f_1(C_b)$, $f_2(T)$, $f_4(\varepsilon,d)$, and $f_5(h)$ are related to the water/cement ratio (w/c) (or reference factor), C_b, temperature T, and relative humidity h, respectively.

Equation (4) should represent a good way to estimate D by accounting for the mentioned factors. Also, Equation (4) should be suitable to the proposed model (explained in Section 3) since it allows the simulation of (i) the external actions of h and T in a variable way, (ii) C_b concentration in the function of C_s, and (iii) the f_3 factor in a dynamic way.

The aging factor, which is directly related with time t, is $f_3(t)$ [40]:

$$f_3(t) = \begin{cases} \frac{1}{1-m}\left(\frac{t_{ref}}{t}\right)^m & \text{If } t < t_r \\ \frac{1}{1-m}\left(\frac{t_{ref}}{t_r}\right)^m & \text{if } t \geq t_r \end{cases} \quad (5)$$

where t_{ref} is the reference concrete age, and t_r is the time after which D is assumed constant. The exponent m is an index that changes with type and quantity of mineral admixtures, and it depends on the fly ash and slag as shown in [41] (here, by neglecting fly ash and slag in concrete, the index m is assumed as m = 0.20). Equation (5) varies in t up to a t_r value and then it maintains constant.

In literature, other factors to estimate D have been introduced. In [11,12] it is considered a factor f(V) to estimate D, which accounts for the volume fraction V and the maximum size of coarse aggregate to quantify the concrete heterogeneity. This factor is not accounted for in this study since the concrete is supposed to be homogeneous. Also, in [15]

a diffusivity relation is shown in function of the volume fractions of recycled aggregate and adhesive rate of mortar.

Figure 2 shows the mentioned factors and their related sub-factors (i.e., parameters of the models). The values for the sub-factors used in this study will be provided in Section 4. These 20 sub-factors can be estimated by specific laboratory tests or retrieved from the literature [16,42–44] (some sub-factors have been already introduced):

- f_0: age, temperature, humidity of concrete; w/c ratio [42].
- f_1: ω_e, α, β, C_f (Equation (6)).
- f_2: E_a is the activation energy of the diffusion process that depends on the type of cement and w/c ratio; R is the universal gas constant that depends on the chemical potential of ions, molar concentration, and temperature [31]; T_0 is the reference temperature [45] (see Section 3.1).
- f_3: t_{ref}, t_r, m (Equation (5)).
- f_4: d, ε and its corresponding load [16]. This factor can be called as "loading factor" and depends on several conditions as the properties of concrete, such as the sinuosity and the shrinkage degree of capillary pores. For this, it is complicated to be estimated as shown in [38,42]. In this paper, it is considered as a constant value.
- f_5: h_c is the humidity, at a certain temperature, at which D drops halfway between its maximum and minimum values; n is a value that characterizes the spread of the drop in D [46] (see Section 3.1).

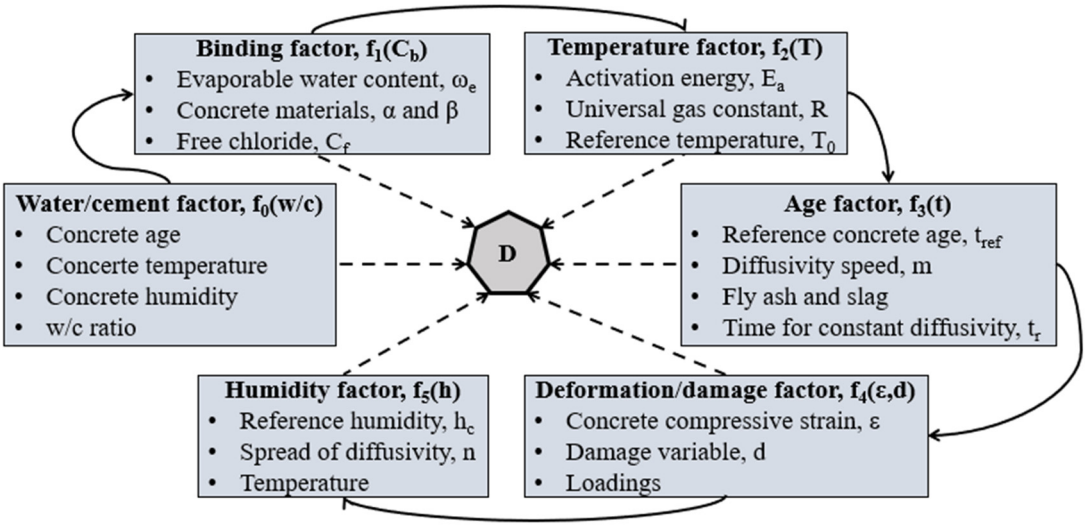

Figure 2. Representation of used 6 factors (from f_0 to f_5) and 20 sub-factors correlated to the chloride diffusion coefficient D.

The total chloride concentration C can be calculated by $C = (\omega - \omega_n)\, C_f + C_b$, where C_f is the free chlorides dissolved in pore solution, C_b is the chemically binding chlorides, and ω is total water content (for $C_b = 0 \rightarrow C = \omega_e\, C_f$). ω can be defined by $\omega = \omega_e + \omega_n$ where ω_e and ω_n are the non-evaporable and evaporable water contents, respectively [44,47].

Given that C_f is mainly transported by water present in the pores of the concrete, it should be reduced by a value of $\omega_e < 1.0$, and thus not contributing to the mechanical diffusion. C_b depends on temperature, cement, and solution types, and includes the reaction/absorption with the solid paste of the cement [48].

C_f can be assumed as $C_f = C_0 + C_s$ since they represent the chloride content present in concrete. Thus, the relationships between C_f and C_b at a known temperature can be estimated by the nonlinear Langmuir isotherms [33,45,49]:

$$f_1(C_b) = \left(1 + \frac{\alpha}{\omega_e(1 + \beta C_f)^2}\right)^{-1} = \left(1 + \frac{\alpha}{\omega_e(1 + \beta(C_0 + C_s))^2}\right)^{-1} \quad (6)$$

where α and β are parameters that depend on the type of concrete. Here, the ordinary Portland concrete is used, and therefore in accordance with the literature [44] the following experimental values are adopted: $\alpha = 11.8$ and $\beta = 4.0$. Equation (6), in this form, assumes a dependency on C_s.

2.2. Numerical Solutions

Numerical solutions allow to pass from analysis with a constant D to a non-constant D. In this way it is possible to account for Equation (4) and propose the model for $C_s{}'$ (see Section 3) for a non-steady state.

For this, Kampé de Fériet (KDFPs) and Hermite (HPs) polynomials are adopted since they have been already used to solve finite element discretization problems as shown in [50] and the Heat equation as shown in [51,52], which has the same form of the second Fick's law.

2.2.1. Constant Diffusivity

Equation (2) for D = 1 has a solution by using the KDFPs of non-negative integers n (i.e., degree of the polynomial), in $x \in R$ and $t \in R$, defined by the series, generating function (with p is an exponential power term) and identity, respectively [39,51,52]:

$$H_n(x,t) = n! \sum_{r=0}^{\left[\frac{n}{2}\right]} \frac{x^{n-(2r)} t^r}{(n-2r)!r!} \quad (7)$$

$$\sum_{n=0}^{\infty} \frac{p^n}{n!} H_n(x,t) = e^{xp+tp^2} \quad (8)$$

$$H_n(x,t) = e^{t\partial^2/\partial x^2}(x^n) \quad (9)$$

Substituting Equation (7) in Equation (2), with the initial and boundary conditions, it is obtained:

$$\begin{cases} \frac{\partial}{\partial t} H_n(x,t) - \frac{\partial^2}{\partial x^2} H_n(x,t) = 0 \\ \text{Initialcondition :} \quad H_n(x,0) = x^n \\ \text{Boundaryconditions :} \quad H_n(0,t) = 0 \\ H_n(\infty,t) \rightarrow \text{Indeterminate} \end{cases} \quad (10)$$

Equation (10) shows that the KDFP provided by Equation (7) satisfies the equilibrium. For this, Equation (7) can be used to plot numerically the concentration C in time t and space x.

2.2.2. Non-Constant Diffusivity

Equation (7) does not represent the exact solution of Equation (2) for $D \neq 1$. However, it can be used to get HPs approximated solution. Thus, HPs in x and t are introduced by the series, generating function and identity, respectively [51,53]:

$$\begin{cases} H_n(x) = n! \sum_{r=0}^{\left[\frac{n}{2}\right]} \frac{(2x)^{n-2r}(-1)^r}{(n-2r)!r!} & \text{in } x-\text{axis} \\ H_n(t) = n! \sum_{r=0}^{\left[\frac{n}{2}\right]} \frac{(2t)^{n-2r}(-1)^r}{(n-2r)!r!} & \text{in time t} \end{cases} \quad (11)$$

$$\begin{cases} \sum_{n=0}^{\infty} \frac{p^n}{n!} H_n(x) = e^{2xp+p^2} & \text{in } x-\text{axis} \\ \sum_{n=0}^{\infty} \frac{p^n}{n!} H_n(t) = e^{2tp+p^2} & \text{in time } t \end{cases} \quad (12)$$

$$\begin{cases} H_n(x) = (-1)^n e^{x^2} \frac{d^n}{dx^n}\left(e^{-x^2}\right) & \text{in } x-\text{axis} \\ H_n(t) = (-1)^n e^{t^2} \frac{d^n}{dt^n}\left(e^{-t^2}\right) & \text{in time } t \end{cases} \quad (13)$$

HPs satisfy the orthogonality relation: $H_n(\cdot)$ and other HPs of degree j, $H_j(\cdot)$, are orthogonal in $L^2{}_\omega(\Lambda)$ where $\Lambda = (-\infty, +\infty)$ with respect to the weight function $\omega(\cdot) = e^{-(\cdot)^2}$ and satisfy in the following relation [53]:

$$\int_{-\infty}^{+\infty} H_n(\cdot) H_j(\cdot) \omega(\cdot) d(\cdot) = 2^n n! \sqrt{\pi} \delta_{n,j} \quad (14)$$

where $\delta_{n,j}$ is the Kronecker delta function assuming Equation (14) is equal to zero for $n \neq j$.

In this study, to solve Equation (2) by considering a non-constant D, the conditions are defined as:

$$\begin{array}{rc} \text{Initial condition :} & C(x_m, 0) = C_0 \\ \text{Boundary conditions :} & C(0, t_m) = C_s \\ & C(q \times x_m, t_m) = C_0 \end{array} \quad (15)$$

where x_m and t_m are two pre-imposed variables related to the position and time, respectively. The parameter q defines the boundary conditions for a finite medium (here is assumed q = 20 in accordance with previous studies [39,43]).

These previous studies [39,43] were useful to validate the use of HPs also in this work. However, in these studies, the proposed model described in Section 3 has not been accounted for, and therefore a comparison with analytical solutions was necessary.

3. Proposed Chloride Ingress Model for Unsaturated Conditions

The proposed model is divided into four phases as shown in Figure 3. The first phase considers the effects of humidity and temperature on the whole diffusion process. The second phase accounts for the effects of concrete irregularities during a building, which should respect specific tolerances for concrete construction and materials [54–56].

In the third phase, it is considered that the maximum chloride concentration $C_s{}'$ is located inside the concrete at the distance x' for non-saturated conditions. Finally, in the fourth phase, the diffusion process by Fick's laws is modeled using the multifactorial numerical approach already presented (Equation (4)) and considering the effects mentioned for phases I, II, and III. In the following sections, each phase is described and justified.

All phases encompass all factors modifying the chloride ingress in the convection area. A physical condition to obtain Equation (3) is that C_s must be uniform and constant in t and x and the external surface of the concrete must be plane [22,57]. This condition could be applied when the effects of the environment variations are negligible and there is no frequent washing for example by rain [40]. However, C_s depends on environmental conditions, topography, the orientation of the concrete surface, and distance from the coastline [1]. In [26] it is also shown that C_s depends on the chloride binding capacity of the concrete and its porosity at the surface, whereas in [4] C_s have correlated to the wind dynamic actions. In this sense, C_s in real conditions are not constant in time t.

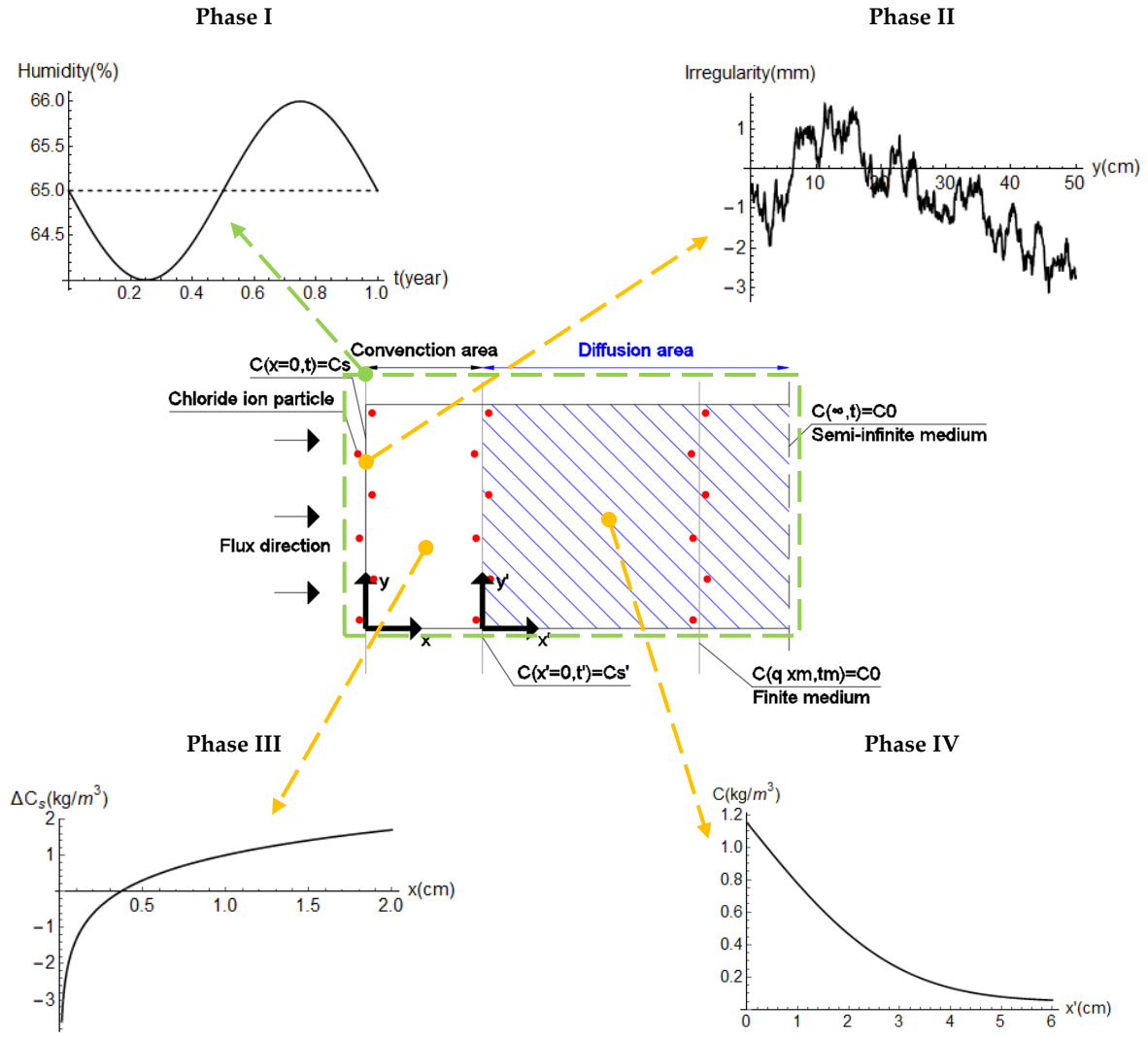

Figure 3. Proposed model (**middle**) and phases: (**above**) environmental conditions and concrete irregularity; (**below**) increment of C_s and diffusion process. The model is composed of two reference systems: x, y, t, and x′, y′, t.

It is more useful for lifetime assessment, to estimate an equivalent surface chloride concentration (C_s') in the boundary between the convection and diffusion zones that are located at the distance x′ from the concrete surface (see Figure 1). Therefore, in this section a new procedure to estimate C_s' under the following hypotheses is proposed:

- Concrete is homogenous and subjected to an atmospheric chloride condition at $x \geq 0$.
- Two different axis systems are defined: x, y, and x′, y′ to differentiate between the convection and diffusion areas (Figure 3).
- Fick's laws (pure diffusion) are only valid for $x' \geq 0$ (diffusion area).
- The diffusion process is unidimensional and is purely mechanical.
- The concrete element is a finite medium described by Equation (15).
- The convection process depends on x-axis.
- D is considered non-constant and multi-factorial.
- The external environment conditions (humidity and temperature) are periodic for a year and vary in t.
- The effects of concrete surface irregularities on C_s are considered.
- There is a difference of C_s, i.e., $\Delta C_s = C_s' - C_s$, from $x = 0$ to $x' = 0$.
- An inner chloride concentration C_0 is considered constant and is added to C_s.

3.1. Phase I: External Environmental Conditions

The external chloride concentration is strongly related to the surrounding environmental conditions where the temperature, humidity, and wind change [4,9]. In [2,3] it is shown how these three parameters influence the chloride concentration in the atmosphere. In this sense, it is possible to consider that external environmental conditions directly affect internal diffusion trends. Therefore, in this phase, the effects of the external relative humidity h and temperature T are considered, which affect the diffusivity D, described in Equation (4), by adding fluctuating trends in time t (expressed in years). The adopted functions $f_2(T)$ and $f_5(h)$ are thus modified as [35]:

$$\begin{cases} f_2(T) \rightarrow g_1(T,\ t) = e^{\left[\frac{E_a}{R}\left(\frac{1}{T_0}-\frac{1}{T(t)}\right)\right]} \\ T(t) = \frac{T_{max}-T_{min}}{2}\sin(2\pi t) + \frac{T_{max}+T_{min}}{2} \end{cases} \quad (16)$$

$$\begin{cases} f_5(h) \rightarrow g_2(h,t) = \frac{1}{1+\frac{(1-h(t))^n}{(1-h_c)^n}} \\ h(t) = -\frac{h_{max}-h_{min}}{2}\sin(2\pi t) + \frac{h_{max}+h_{min}}{2} \end{cases} \quad (17)$$

where T_{max} and T_{min} are respectively the maximum and minimum temperatures in one year, and h_{max} and h_{min} are respectively the maximum and minimum relative humidities in one year. The other parameters in Equations (16) and (17) have been already explained in Section 2.1.

In [35] a periodic function is used where the trend represents the season weather, e.g., one year (t = 1 year) corresponds to one cycle with two peaks: positive (hot and dry summer) and negative (cold and wet winter). Equations (16) and (17) represent these conditions as shown in Figure 4 for the values given in Section 4.1. Therefore, the form of Equations (16) and (17) have been defined *a posteriori*.

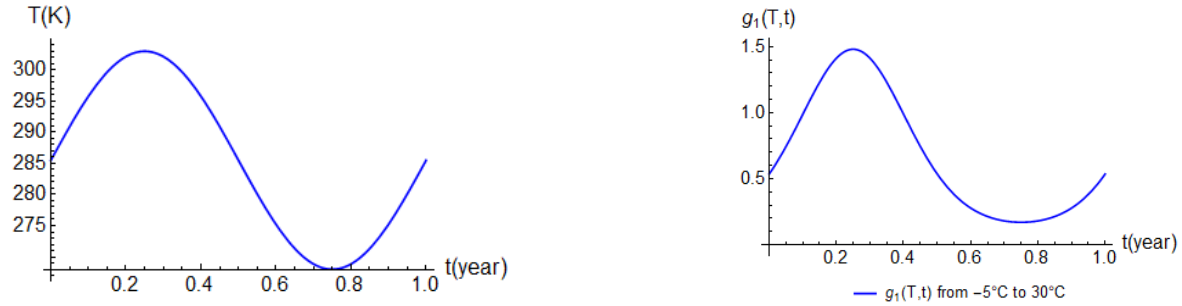

(**a**) Temperature trends

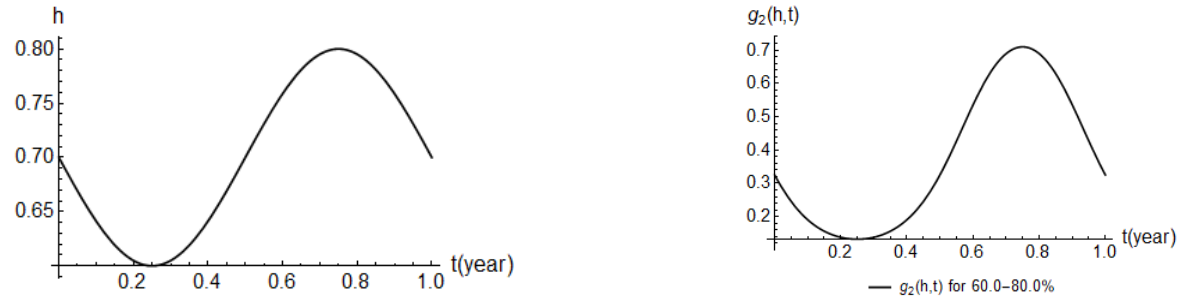

(**b**) Humidity trends

Figure 4. Function trends described by (**a**) Equation (16) and (**b**) Equation (17).

3.2. Phase II: Surface Concrete Irregularities

The goal of this phase is to estimate the variations of C_s in the function of the irregularity trend of the concrete surface, $C_{s,r}$. These irregularities are due to the composition of the concrete, size of aggregates, treatments of concrete smoothing as well as on concrete casting.

In a similar way to a study of pavement irregularities [58], here the concrete surface and the concrete/chloride contact have been defined as a stationary stochastic process described by power spectrum density (PSD) functions $S(\Omega_n)$:

$$S(\Omega_n) = S(\Omega_0)\left(\frac{\Omega_n}{\Omega_0}\right)^{-2} \tag{18}$$

where Ω_n is the spatial frequency, $S(\Omega_0)$ is the irregularity coefficient, and Ω_0 ($\Omega_0 = 0.01\ m^{-1}$) is a reference spatial frequency. The value for $S(\Omega_0)$ depends on the concrete condition; therefore, by considering as worst-case scenario, for a maximum amplitude of the formed surface irregularity of about ± 0.15 cm, as suggested in [54], $S(\Omega_0)$ is assumed *a posteriori* equal to $100\ m^3/rad$.

An irregularity profile r(y) can be generated as the sum of a number (here N = 1500) of harmonic series through the following expression:

$$r(y) = \sum_{n=0}^{N} \sqrt{2S(\Omega_n)\Delta\Omega}\cos(2\pi\Omega_n y + \phi_n) \tag{19}$$

where ϕ_n are the random phase angles distributed in the range 0 to 2π and, $\Delta\Omega$, with $\Omega_f = 10\ m^{-1}$, is:

$$\Delta\Omega = \frac{\Omega_f - \Omega_0}{N} \tag{20}$$

Figure 5 shows a trend of an irregularity profile r(y) at the surface (x = 0), and at the transposed ideal surface (x′ = 0) inside the concrete, i.e., $r(y) + \overline{\Delta x}$, where $\overline{\Delta x}$ is the average difference between the positions of the peak chloride concentration at x′ and x (x is the depth at which C_s is determined). This average value is determined from experimental data as illustrated in Section 3.3.

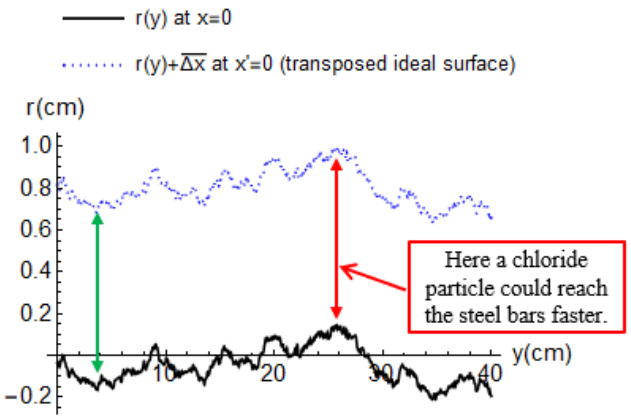

Figure 5. Concrete irregularity trends at x = 0 and x′ = 0 in y-axis.

This trend represents a possible profile, since, as mentioned, Equation (19) generates random profiles. However, given that for each profile the mean value of r(y) is different to zero (i.e., $\overline{r(y)} \neq 0$), it makes sense to consider the contribution of r(y).

By considering the average variation between C_s‘ and C_s (i.e., $\overline{\Delta C_s} = C_s' - C_s$), $C_{s,r}$ is computed as:

$$C_{s,r} = \frac{\overline{\Delta C_s} \times r(y)_{max}}{\overline{\Delta x}} \tag{21}$$

In Section 3.3 will be provided some examples of $\overline{\Delta x}$ and $\overline{\Delta C_s}$ estimated from several collected experimental data. $C_{s,r}$ will be integrated afterward for the assessment of C_s' in Section 3.3.

3.3. Phase III: Changes on C_s Due to Unsaturated Conditions

In this phase, a convection area is considered where C_s increase up to reach a peak value C_s' located in the internal border of the convection zone x'. The convection area, as defined in [20,31], appears under "non-saturated conditions". The diffusion in this region depends on external environmental conditions (e.g., rain, tidal cycles, environmental temperature, relative humidity, solar radiation, etc.) [59].

In the simplified approach by Equation (3), this phase is not considered, i.e., it is assumed that $C_s = C_s'$, which could be directly estimated from information available in Table 1. Table 1 lists four levels of environmental aggressiveness (from low to extreme), which are related to different exposure classes of structures [60,61]. These values are in accordance with those found in [2,3]. Another high condition is added to Table 1, i.e., de-icing salts attack, for structures placed in mountain zones [9,10].

Table 1. Value of C_s for each level of aggressiveness (adapted from [60,61]).

Level of Aggressiveness	Description	C_s (kg/m^3)
Low	Structures placed at ≥2.84 km from the coast. Seaspray coming from the wind is the main source of chlorides [a].	0.35
Moderate	Structures placed between 0.10–2.84 km from the coast without direct contact with seawater.	1.15
High	Structures placed to ≤0.10 km from the coast without direct contact with seawater.	2.95–3.50 [b]
Extreme	Structures subject to wetting/drying cycles. The processes of chloride accumulation are due to seawater, evaporation, salt crystallization.	7.35

[a] At 4.50 km from the coast, C_s can also reach high values due to the combination among T, h, and wind as shown in [3]. [b] 3.50 kg/m^3 refers to an inland structure located in a cold region where de-icing salts are applied during a winter period [9].

From literature [13,25–30], 136 values have been collected to determine C_s' at x'. The main selection criterium is related to unsaturated exposure conditions where the chloride concentration profiles reach a maximum value C_s' at x' point. The collected values come from several results plotted in chloride concentration vs. concrete depth curves shown in each paper. In this sense, it was possible to estimate the points that correspond to C_s, C_s', x, and x' values.

All values have been homogenized for comparison purposes since in some studies [13,26] C_s is expressed in different units. These values were obtained from (1) laboratory measurement tests and (2) real structure monitoring. All studied element sizes can be different; however, the diffusion model is unidimensional; and therefore, it is supposed that the size of the concrete components is enough to ensure chloride ingress in one dimension.

All data refer to the same type of ordinary Portland concrete. The main considered conditions are summarized as follows:

1. For laboratory tests: 1 month of exposure time under the mean values of T = 20 °C and h = 60.0% [29]; 14 days of exposure time under dry/wet cycles (extreme level of aggressiveness) [28]; 8 weeks of exposure time [30]; 60 months of exposure time in the tidal zone (extreme level of aggressiveness) [13].
2. For real structures: 12–16 years of field exposure time [27]; 25 years of service life in marine environments under the mean values of T = 27 °C and h = 70.8% [26]; 28 years of exposure time under the mean values of T = 12.8 °C and h = 80.0 % [25].

Figure 6 shows the collected values of C_s at depth x (Figure 6a) and C_s' at depth x′ (Figure 6b), indicating the four levels of aggressiveness (horizontal lines) from low to extreme in accordance with Table 1.

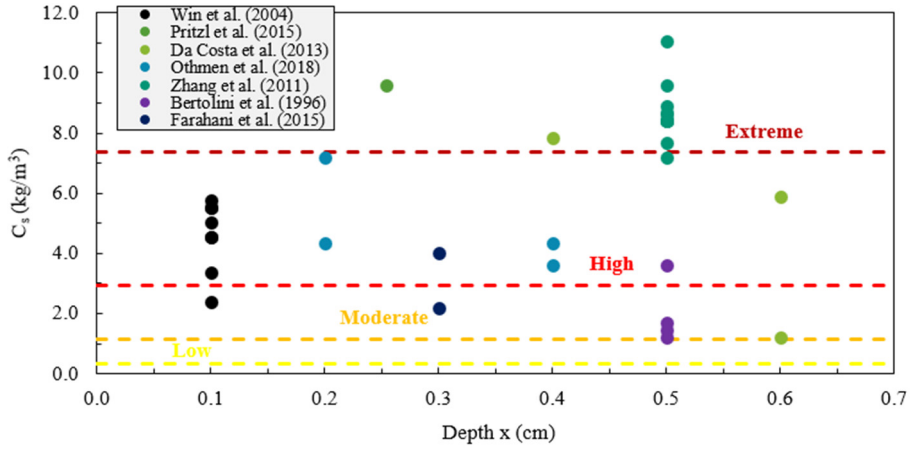

(**a**)

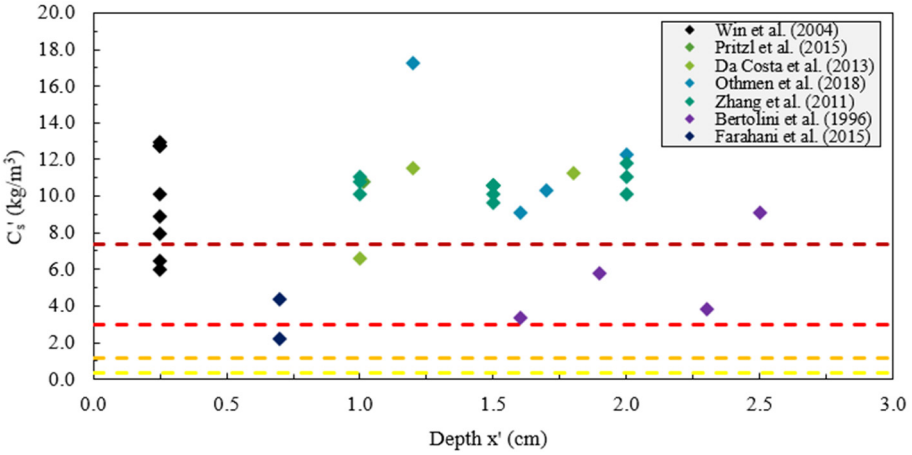

(**b**)

Figure 6. Collected data: (**a**) C_s at depth x and (**b**) C_s' at depth x′ retrieved from literature [13,25–30]. The horizontal lines indicate the four levels of aggressiveness (from low to extreme, Table 1).

From points shown in Figure 6, the registered maximum and minimum values of C_s are 11.04 kg/m^3 (at x = 0.50 cm) and 1.20 kg/m^3 (at x = 0.50 cm), respectively, whereas the registered maximum and minimum values of C_s' are 17.28 kg/m^3 (at x′ = 1.20 cm) and 2.20 kg/m^3 (at x′ = 0.70 cm), respectively.

The depth x and x′ range between 0.10 to 0.60 cm and 0.25 to 2.50 cm, respectively. Here, it is possible to note that C_s values do not reach the maximum values at x = 0 where they should be expected. This should be correlated to the fact that during the measurements, the chloride ions are generally extracted at a given depth $x \neq 0$.

All collected data have been processed and studied. First, we determine the differences of the chloride concentrations and related depths between the surface and the boundary of convection and diffusion zones. Then, we estimate the mean value and its standard deviation, σ. Table 2 shows the results for each collected parameter by considering the following range: low (0–1.14 kg/m^3), moderate (1.15–2.94 kg/m^3), high (2.95–7.34 kg/m^3), and extreme (>7.35 kg/m^3) levels of aggressiveness. As expected, larger values of C_s, C_s', and Δx (= x′ − x) were found for larger levels of aggressiveness.

Table 2. C_s, C_s', ΔC_s, and Δx values for each level of aggressiveness [a].

Parameter	Level of Aggressiveness	Unit	Number of Measures	Mean	σ
C_s	Low	kg/m^3	–	–	–
	Moderate		6 (see Figure 6a)	1.69	0.50
	High		15 (see Figure 6a)	4.96	1.21
	Extreme		13 (see Figure 6a)	8.76	0.88
C_s'	Low	kg/m^3	–	–	–
	Moderate		1 (see Figure 6b)	N/A	N/A
	High		7 (see Figure 6b)	5.21	1.32
	Extreme		26 (see Figure 6b)	10.91	1.78
ΔC_s [b]	Low	kg/m^3	–	–	–
	Moderate		6	3.84	3.53
	High		15	5.10	2.78
	Extreme		13	1.87	0.85
Δx	Low	cm	–	–	–
	Moderate		6	0.91	0.63
	High		15	0.68	0.65
	Extreme		13	1.01	0.38

Note: N/A = Not available. [a] Rigorously, this classification should be possible only for C_s values in accordance with the criteria used in Table 1, but, to obtain an order of aggressiveness of the Cs', ΔC_s, and Δx impact, for these values the classification is also made. [b] This parameter has been divided in the function of the level of aggressiveness of C_s values to quantify their increments in $x' - x$.

Finally, from Equation (15), the boundary condition regarding C_s at $x' = 0$ for the numerical analyses, C_s', will be defined by the following function:

$$C_s'\left(x' = 0\right) = C_s + \Delta C_s + C_{s,r} \tag{22}$$

With respect to Equation (21), Equation (22) also integrates the contribution of C_s increment in convection area, ΔC_s, in the numerical analyses.

3.4. Phase IV: Chloride Ion Diffusion

In this last phase, the chloride ion diffusion is developed by Fick's laws. Three conditions have been defined to quantify the possible variations of C_s' that represent the peak of the diffusion profile:

$$\begin{cases} C_s' > C_s & \text{Upper limit} \\ C_s' = C_s & \text{Standard limit} \\ C_s' < C_s & \text{Lower limit} \end{cases} \tag{23}$$

The increment of standard C_s is quantified as $C_s + \Delta C_s = C_s'$, where the upper limit is verified when $\Delta C_s > 0$, whereas the lower limit is verified when $\Delta C_s < 0$. In these situations, there is an accumulation or reduction of chloride ions in concrete, respectively. The standard limit regards the case where the convection area is not considered (i.e., $\Delta C_s = 0$) as, for instance, for chloride ions immersion as mentioned in [20,31].

4. Numerical Examples

4.1. Problem Description and Used Materials

This section summarises the problem description and data used for the analyses. As shown in Table 3, some data have been collected from the literature for concrete produced by using ordinary Portland cement.

Table 3. Used parameters and their values.

Parameter	Value and reference
Inner chloride concentration, C_0	0.50 kg/m^3 [62]
Surface chloride concentration, C_s	(see Table 1)
Reference factor, $f_0(w/c)$	4.35 cm^2/year [42] [a]
Binding factor, $f_1(C_b)$	0.85–0.93 (Equation (6)) [b]
Age factor, $f_3(t)$	0.38–0.75 (Equation (5)) [c]
Deformation/damage factor, $f_4(\varepsilon,d)$	1.73 [38]
Modified temperature factor, $g_1(T,t)$	0.17–1.48 (Equation (16)) [d]
Modified humidity factor, $g_2(h,t)$	0.13–0.71 (Equation (17)) [e]
Constant diffusivity, D	0.47 cm^2/year (Equation (4)) [f]

[a] With w/c = 0.50 (ordinary Portland cement). [b] For $C_f = C_0 + C_s$ = 0.85–7.85 kg/m^3, and ω_e = 0.14 [47]. Other values are shown in Equation (6). [c] For t = 1.0–30.0 years. With m = 0.20, t_{ref} = 0.08 years (= 28 days), and t_r = 30.0 years [41]. [d] With E_a = 41.8 kJ/mol, R = 8.314 J/mol K, T_0 = 296.0 K [16], and T = 268.0–303.0 K (i.e., from about −5.0 to +30.0 °C). [e] For h = 0.60–0.80, n = 0.40, and h_c = 0.75 [7]. [f] This value is obtained considering the mean constant values of each factor by using Equation (4).

The used values of the environmental conditions described in the phase I range between −5 to 30 °C (temperature) and 60 to 80% (humidity). As already explained, it is assumed that the external environmental conditions (temperature and relative humidity) also maintain the same inside the concrete. This approximation could lead to some errors, especially when assessing the water content inside the concrete.

The f_4 factor accounts for the possibility to amplify the diffusivity of the chloride ions due to the concrete cracks [63]. Here an experimental value has been adopted, which refers to "load-induced cracks" under "static loading" [38].

In Table 3 it is possible to see the weight of each factor. In particular, it is evident how the factors f_0, f_4, and g_1 play important roles in the increase of diffusivity D since they can reach a value >1.0. In this sense and favor of safety, one could state that other factors and their correlated sub-factors (Figure 2) could be neglected. This aspect has been treated in another study [39].

Figure 7a shows the trend of the factors in time t described in Equation (4) using the values in Table 3. The factors f_0, f_1, and f_4 are not dependent on time; therefore, they are plotted by a unique constant horizontal line (dashed line). The sinusoidal trends are due to the function g_1 and g_2 described in Equations (16) and (17), respectively. Finally, the exponential trend is due to the factor f_3 defined in Equation (5) where for $t_r \geq 30$ years this factor assumes a constant value. In Figure 7a the weight of the g_1 factor (see "$f_0 \times g_1$" grey curve) is more evident since it varies between a great range of −5 to 30 °C strongly affecting the diffusivity. However, this effect is damped by the g_2 factor (see "$f_0 \times g_1 \times g_2$" red curve) that re-balances the diffusivity; as shown in Figure 4, when T is maximum (hot weather) the humidity is minimum (dry weather), and vice-versa. The exponential decrease of the f_3 factor due to concrete aging is also observed (see "$f_0 \times f_3$" yellow curve).

Figure 7b depicts the trends of the non-constant and constant values of diffusivity D (= 0.47 cm^2/year, Table 3), used in the analyses, considering all factors, their interdependencies, interactions, and fluctuations. In Figure 7b it is possible to see the difference between the constant and non-constant multifactorial values of D. Up to ~5 years the non-constant D is higher than the constant D and therefore the chloride concentration in RC structures by using analytical solutions with the constant D (Equation (3)) could be under-estimated. After ~15 years, an overestimation of the chloride ingress rate in the case of the constant D could lead to wrong lifetime assessments.

Therefore, the use of a non-constant multifactorial D allows estimating the chloride concentration accounting for external and internal factors, that affect the structural concrete and the diffusion mechanical process to provide several more reliable predictions.

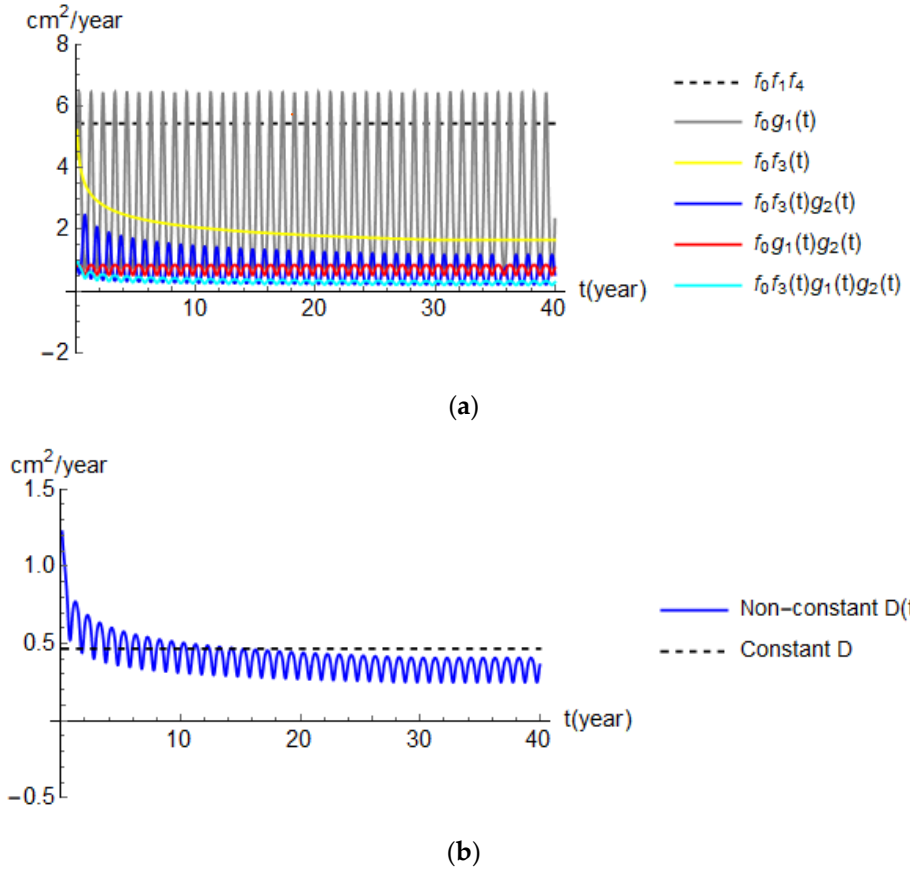

Figure 7. Diffusivity: (**a**) factor trends with respect to the reference constant f_0 factor; (**b**) non-constant and constant D with all factors.

4.2. Description of Analysed Cases

This paper considers and compares four cases identified by four specific line types on the next results:

1. Solid black line: analytical results by using Equation (3) with a constant D. This analysis is used to compare the numerical analyses and the proposed model. The used D is 0.47 cm^2/year (Table 3), and the C_s values are shown in Table 1.
2. Dashed black line: analytical results like the previous case plus the contribution of C_s'. In this case, it is possible to see the impact of the convection area where C_s increases (grey area) and the effects of the non-constant D.
3. Dashed blue line: numerical results by Equation (11) considering the non-constant multifactorial D and the proposed model shown in Figure 3. Due to the amplitude of the irregularity profile, an upper curve and a lower curve are plotted, which represent the chloride contents for the $r(y)_{max}$ and $r(y)_{min}$, respectively. Therefore, the effects of the irregularity are represented by the filled blue area. For each analysis, a different irregularity profile is generated, but its random variability is imperceptible since $\overline{r(y)}$ maintains substantially constant.
4. Solid orange line: numerical results like analysis 3 but without the irregularity effects (i.e., $r(y) = 0$).

For these 4 analyses developed by Mathematica software [64], the high and extreme levels of aggressiveness have been considered since, as shown in Table 2, the most significant data regard these levels. However, the information about the conditions on the data (listed in Section 3.3) shows that most of the data come from the conditions subjected to an extreme level of aggressiveness and/or a long period of exposure. This means that 21 data of C_s classified as "moderate/high level" could be not consistent. This indicates that it is

very difficult to define the history of the external conditions that act on the structure by knowing only *a posteriori* C_s values. For this, a unique value of $\overline{\Delta C_s}$ = 3.64 kg/m^3, which is the mean of all data, is used for both high and extreme aggressiveness cases. In this sense, by Equation (23), the upper limit case is always verified.

4.3. Results

Figures 8 and 9 show the chloride ion concentration C in concrete in the function of x' axis and time t. Periods of 5, 10, 35, and 50 years and x' varying between 0 and 6 cm have been considered. The boundaries of the numerical solutions indicated in Equation (15) are calculated within an interval of $0 < t_m \leq 50$ years and $0 \leq x_m \leq 6$ cm.

As expected, the results in Figure 8, provide higher values for extreme aggressiveness than for high aggressiveness. For example, at x' = 3.50 cm (i.e., $x + \overline{\Delta x} = 3.50 + 0.85 = 4.35$ cm) where steel bars should be placed, the difference of C comparing both aggressiveness levels and all times varies around 2.0 for all models.

In Figure 8, the analytical model gives lower concentrations than the numerical ones mainly due to the difference of $\overline{\Delta C_s}$ as expected in the theory (see Figure 1). This difference of $\overline{\Delta C_s}$ = 3.64 kg/m^3 is maintained constant at x' = 0 but it affects the chloride C in a different way depending on the used model.

It is important to say that for the case of saturated exposure described by the analytical cases, the existence of the convection zone is not accounted, leading, in this case, to an underestimation of chloride concentrations.

The influence of the surface concrete irregularity is shown by the filled blue area. The numerical solutions without considering the irregularity, i.e., r(y) = 0 (orange line), pass in the center of the filled area; in this sense, the orange line represents the mean value. The upper chloride bound of the filled blue area represents the case when a chloride ion is closer to the steel rebar because of larger irregularities that decrease concrete cover; therefore, in this case, it should reach a steel bar faster and vice-versa as indicated in Figure 5. It is also observed that the reduction of the filled area with the increasing of depth x', indicating that there is a decrease in the influence of irregularities with depth. These numerical results highlight that the effects of surface regularities should be experimentally validated in further studies to improve lifetime assessment.

In Figure 9 the impact of the presence of the convection area is highlighted by the solid grey area where two limits are defined by the analytical solutions. The lower bound corresponds to an analytic model with the constant D, whereas the upper bound considers an analytic model by also accounting for the presence of the convection zone. It is observed in all considered cases that there is an underestimation of the chloride concentration C when convection is neglected. The differences decrease for larger depths and times. These results suggest that ΔC_s, due to the presence of a convection area, should be considered to improve lifetime assessment.

The effect of the non-constant multifactorial D is shown in Figure 9. It is represented by the difference between the numerical curve (orange) and the analytical curve (dashed black line) because both models account for the presence of a convection area, and therefore, at x' = 0 the concentration C is the same. These differences are consistent with Figure 7b where the non-constant D is higher than a constant D from a certain exposure time, producing high chloride concentrations for a relatively short period (t < 10 years). This is confirmed in Figure 9a where at $t \approx 10.0$ years both curves intersect each other.

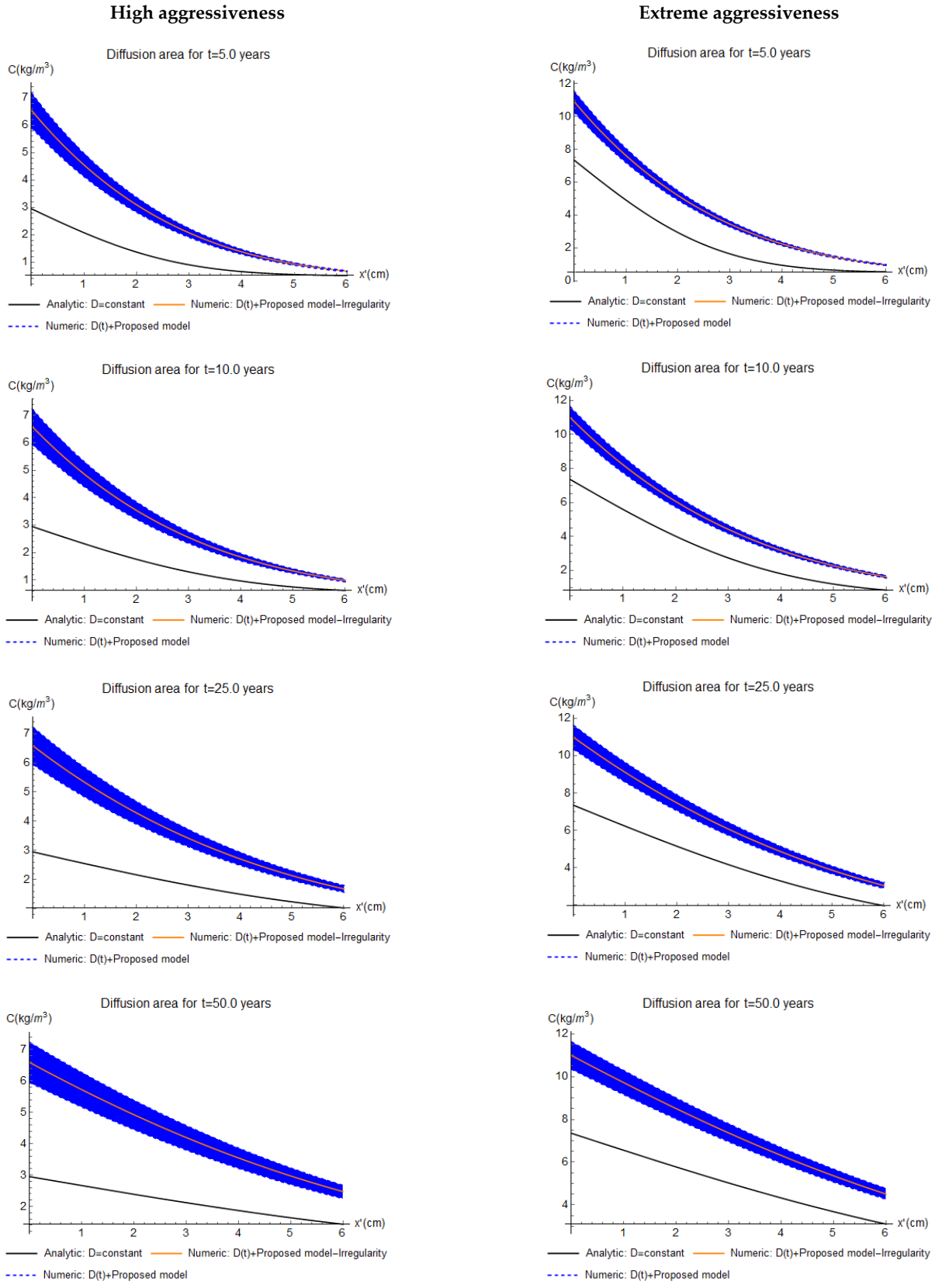

Figure 8. C-x′ curves by analytical and numerical solutions for (**a**) high and (**b**) extreme levels of aggressiveness.

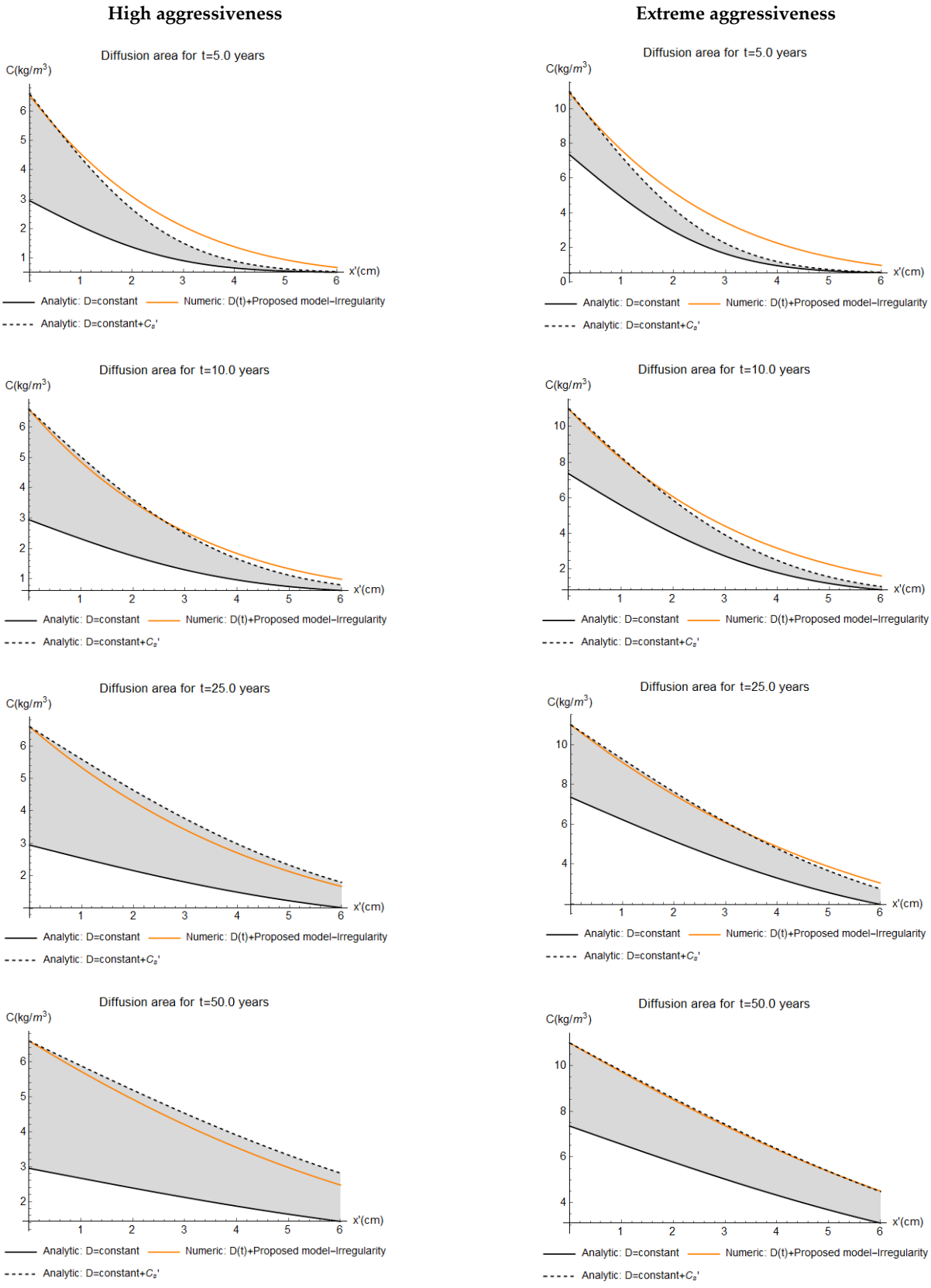

(**a**) (**b**)

Figure 9. C-x′ curves by analytical and numerical solutions for (**a**) high and (**b**) extreme levels of aggressiveness.

In this sense, it is possible to state that analytical solutions underestimate the chloride concentration C for the period t < 10 years and overestimate C for t > 10 years. This is mainly due to the absence of the variability of the factors g_1, g_2, and f_3 for the constant D. However, this consideration is not always verified. In fact, in Figure 9b for $x' > 5.0$ cm, the numerical curve is always higher than the analytical curve, and therefore in this case the analytical solutions also underestimate the concentrations C. This is due to the reduction of C_s' effects that is more evident for higher depths.

The uniqueness of these results mainly regards the use of the proposed model in Figure 3 and the trend of the non-constant D shown in Figure 7b.

To the best of the authors' knowledge, there are no similar models that account uniquely for the concrete irregularity and the increment of C_s. Therefore, it was difficult to compare our model with other studies. However, the following aspects were conducted to validate it: (i) the use of consolidated inputs adopted in several published studies (see Tables 1 and 3); (ii) the use of numerical analyses already calibrated in previous studies, e.g., [39,43]; (iii) the collection of data from reliable published studies (see Figure 6 and Table 2); and (iv) the comparison of the error function based solutions with the new numerical results in this paper.

5. Conclusions

This paper proposed a new model to study the chloride ingress in an RC element in a non-saturated area. It accounts for non-constant diffusivity, surface concrete irregularity, and the presence of a convention area. The main conclusions are summarized as follows:

- The diffusivity D, which is the key parameter of the mechanical diffusion process, should account for the w/c ratio, chloride binding, variations of temperature and humidity, concrete aging, concrete deformation, and damage. This paper used a new complete multi-factorial D (Equation (4)) that includes 20 sub-factors to estimate in a more realistic way the chloride ingress process. It is shown that up to ~10 years the non-constant D is higher than the constant D, and therefore, the chloride concentration in RC structures by using a constant D could be underestimated. After ~15 years the situation is the opposite; however, an underestimation of the chloride attack for the early service life could increase corrosion initiation risks.
- From literature, 136 values have been collected to find two parameters characterizing the convection zone ($\overline{\Delta C_s}$ and $\overline{\Delta x}$). Both parameters were integrated into the proposed multi-phase model (see Figure 3) to estimate the evolution of chloride concentration inside non-saturated concrete. From the results of the numerical example, it is possible to affirm that the consideration of convection effects is crucial to improve the accuracy of the prediction models. Further research will focus on the experimental validation of the proposed approach.
- Numerical solutions by using HPs have been carried out to develop the proposed model in a dynamic way. Due to the variability of some factors and parameters, only by advanced numerical solutions, it could be possible to plot good approximations of chloride concentrations in concrete. The results show that the analytical solutions could underestimate the chloride concentration C for period t < 10 years and for $x' > 4.0$ cm.

Finally, to the best of the authors' knowledge, in literature, there are no similar models that account, as proposed herein, for surface concrete irregularity and the increment of C_s in the convection area. Therefore, we have no available experimental results to compare and validate our model at this stage of our research.

Based on the results of this study we hope in the future to design and carry out an experimental campaign allowing us to compare and validate our proposed model. In addition, further research will focus on the application to other concrete formulations. This will require new experiments to provide all the model parameters and chloride profiles to study how this model behaves for other concrete formulations.

Author Contributions: Conceptualization, E.Z.; methodology, E.Z. and E.B.-A.; software, E.Z.; validation, E.B.-A. and E.Z.; formal analysis, E.Z.; investigation, E.Z. and E.B.-A.; data curation, E.Z. and E.B.-A.; writing-original draft preparation, E.Z.; writing-review and editing, E.B.-A. and E.Z. All authors have read and agreed to the published version of the manuscript.

Funding: E.B.-A. contribution was carried out in the framework of the Strengthening the Territory's Resilience to Risks of Natural, Climate and Human Origin (SIRMA) project, which is co-financed by the European Regional Development Fund (ERDF) through INTERREG Atlantic Area Program with application code: EAPA_826/2018. The sole responsibility for the content of this publication lies with the author. It does not necessarily reflect the opinion of the European Union. Neither the INTERREG Europe program authorities are responsible for any use that may be made of the information contained therein.

Institutional Review Board Statement: Not applicable.

Informed Consent Statement: Not applicable.

Data Availability Statement: The data that support the findings of this study are available from the corresponding author, E.Z., upon reasonable request.

Acknowledgments: E.Z. acknowledges Itecons institute, Coimbra, Portugal, for the Wolfram Mathematica license and University of Coimbra (UC), Portugal, to pay the rights (when applicable) to completely download all papers in the references. The authors also acknowledge the 6 anonymous peer-reviewers for their suggestions and comments.

Conflicts of Interest: The authors declare no conflict of interest.

References

1. Meira, G.R.; Andrade, M.C.; Padaratz, I.J.; Alonso, M.C.; Borba, J.C., Jr. Measurements and modelling of marine salt transportation and deposition in a tropical region in Brazil. *Atmos. Environ.* **2006**, *40*, 5596–5607.
2. Valdes, C.; Castañeda, A.; Corvo, F.; Marrero, R.; Montero, R. Atmospheric corrosion study of carbon steel in Havana waterfront zone. In *Proceedings of the International Conference of Sustainable Production and Use of Cement and Concrete, Villa Clara, Cuba, 23–30 June 2019*; Martirena-Hernandez, J., Alujas-Díaz, A., Amador-Hernandez, M., Eds.; RILEM Bookseries; Springer: Cham, Switzerland, 2020.
3. Guerra, J.C.; Castañeda, A.; Corvo, F.; Howland, J.J.; Rodriguez, J. Atmospheric corrosion of low carbon steel in a coastal zone of Ecuador: Anomalous behaviour of chloride deposition versus distance from the sea. *Mater. Corros.* **2019**, *70*, 444–460. [CrossRef]
4. Ou, Y.C.; Fan, H.D.; Nguyen, N.D. Long-term seismic performance of reinforced concrete bridges under steel reinforcement corrosion due to chloride attack. *Earthq. Eng. Struct. Dyn.* **2013**, *42*, 2113–2127. [CrossRef]
5. Neville, A.M. *Properties of Concrete*, 5th ed.; Pearson Education: Essex, UK, 2011.
6. Val, D.V.; Stewart, M.G. Life-cycle cost analysis of reinforced concrete structures in marine environments. *Struct. Saf.* **2003**, *25*, 343–362. [CrossRef]
7. Bentz, D.P.; Detwiler, R.J.; Garboczi, E.J.; Halamickova, P.; Schwartz, L.M. Multi-scale modelling of the diffusivity of mortar and concrete. In Proceedings of the Chloride Penetration into Concrete, RILEM (1997), Saint-Rémy-lès-Chevreuse, France, 15–18 October 1995; pp. 1–6.
8. Ye, H.; Fu, C.; Jin, N.; Jin, X. I nfluence of flexural loading on chloride ingress in concrete subjected to cyclic drying-wetting condition. *Comput. Concr.* **2015**, *15*, 183–199. [CrossRef]
9. Nguyen, P.T.; Bastidas-Arteaga, E.; Amiri, O.; El Soueidy, C.P. An efficient chloride ingress model for long-term lifetime assessment of reinforced concrete structures under realistic climate and exposure conditions. *Int. J. Concr. Struct. Mater.* **2017**, *11*, 199–2013. [CrossRef]
10. Ghods, P.; Karadakis, K.; Isgor, O.B.; McRae, G. Modeling the Chloride-Induced Corrosion Initiation of Steel Rebar in Concrete. In Proceedings of the COMSOL Conference, Boston, MA, USA, 8–10 October 2009.
11. Wang, Y.; Wu, L.; Wang, Y.; Liu, C.; Li, Q. Effects of coarse aggregates on chloride diffusion coefficients of concrete and interfacial transition zone under experimental drying-wetting cycles. *Constr. Build. Mater.* **2018**, *185*, 230–245. [CrossRef]
12. Wu, L.; Wang, Y.; Wang, Y.; Ju, X.; Li, Q. Modelling of two-dimensional chloride diffusion concentrations considering the heterogeneity of concrete materials. *Constr. Build. Mater.* **2020**, *243*, 118213. [CrossRef]
13. Farahani, A.; Taghaddos, H.; Shekarchi, M. Prediction of long-term chloride diffusion in sílica fume concrete in a marine environment. *Cem. Concr. Compos.* **2015**, *59*, 10–17. [CrossRef]
14. Ying, J.; Jiang, Z.; Xiao, J. Synergist effects of three-dimensional graphene and silica fume on mechanical and chloride diffusion properties of hardened cement past. *Constr. Build. Mater.* **2022**, *316*, 125756. [CrossRef]
15. Ying, J.; Zhou, B.; Xiao, J. Pore structure and chloride diffusivity of recycled aggregate concrete with nano-SiO_2 and nano-TiO_2. *Constr. Build. Mater.* **2017**, *150*, 49–55. [CrossRef]

16. Zacchei, E.; Nogueira, C.G. Chloride diffusion assessment in RC structures considering the stress-strain sate effects and crack width influences. *Constr. Build. Mater.* **2019**, *201*, 100–109. [CrossRef]
17. Nogueira, C.G.; Leonel, E.D.; Coda, H.B. Probabilistic failure modelling of reinforced concrete structures subjected to chloride penetration. *Int. J. Adv. Struct. Eng.* **2012**, *4*, 10–23. [CrossRef]
18. De Rincón, O.T.; Castro, P.; Moreno, E.I.; Torres-Acosta, A.A.; De Bravo, O.M.; Arrieta, I.; García, C.; García, D.; Martínez-Madrid, M. Chloride profiles in two marine structures-meaning and some predictions. *Build. Environ.* **2004**, *39*, 1065–1070. [CrossRef]
19. Rahimi, A.; Gehlen, C. Semi-probabilistic approach to the service life design of reinforced concrete structures under chloride attack. *Beton.-Und. Stahlbetonbau.* **2018**, *113*, 13–21. [CrossRef]
20. Liu, J.; Liu, J.; Huang, Z.; Zhu, J.; Liu, W.; Zhang, W. Effect of fly ash as cement replacement on chloride diffusion, chloride binding capacity, and micro-properties of concrete in a water soaking environment. *Appl. Sci.* **2020**, *10*, 6271. [CrossRef]
21. Liu, J.; Ou, G.; Qiu, Q.; Chen, X.; Hong, J.; Xing, F. Chloride transport and microstructure of concrete with/without fly ash under atmospheric chloride condition. *Constr. Build. Mater.* **2017**, *146*, 493–501. [CrossRef]
22. Silva, C.A.; Guimarães, A.T.C. Evaluation of the diffusion model considering the variation in time of the chloride content of the concrete surface. *Matéria* **2014**, *19*, 81–93.
23. Crank, J. *The Mathematics of Diffusion*; Oxford University Press: Oxford, UK, 1975; p. 421.
24. Pang, L.; Li, Q. Service life prediction of RC structures in marine environment suing long term chloride ingress data: Comparison between exposure trials and real stricture surveys. *Constr. Build. Mater.* **2016**, *113*, 979–987. [CrossRef]
25. Othmen, I.; Bonnet, S.; Schoefs, F. Statistical investigation of different analysis methods for chloride profiles within a real structure in a marine environment. *Ocean Eng.* **2018**, *157*, 96–107. [CrossRef]
26. Da Costa, A.; Fenaux, M.; Fernández, J.; Sánchez, E.; Moragues, A. Modelling of chloride penetration into non-saturated concrete: Case study application for real marine offshore structures. *Constr. Build. Mater.* **2013**, *48*, 217–224. [CrossRef]
27. Pritzl, M.D.; Tabatabai, H.; Ghorbanpoor, A. Long-term chloride profiles in bridge decks treated with penetrating sealer or corrosion inhibitors. *Constr. Build. Mater.* **2015**, *101*, 1037–1046. [CrossRef]
28. Zhang, S.F.; Lu, C.H.; Liu, R.G. Experimental determination of chloride penetration in cracked concrete beams. *Procedia Eng.* **2011**, *24*, 380–384.
29. Win PPWatanabe, M.; Machida, A. Penetration profile of chloride ion in cracked reinforced concrete. *Cem. Concr. Res.* **2004**, *34*, 1073–1079.
30. Bertolini, L.; Bolzoni, F.; Elsener, B.; Pedeferri, P.; Andrade, C. La realcalinizacion y la extraccion electroquimica de los cloruros en las construcciones de hormigon armado. *Mater. De Constr.* **1996**, *46*, 1–12. [CrossRef]
31. Zofia, S.; Adam, Z. Theoretical model and experimental tests on chloride diffusion and migration processes in concrete. *Proc. Eng.* **2013**, *57*, 1121–1130. [CrossRef]
32. Carrara, P.; De Lorenzis, L.; Bentz, D.P. Chloride diffusivity in hardened cement paste from microscale analyses and accounting for binding effects. *Model. Simul. Mat. Sci. Eng.* **2016**, *24*, 065009. [CrossRef]
33. Sun, Y.M.; Liang, M.T.; Chang, T.P. Time/depth dependent diffusion and chemical reaction model of chloride transportation in concrete. *App. Math. Mod.* **2012**, *36*, 1114–1122. [CrossRef]
34. Suo, Q.; Stewart, M.G. Corrosion cracking prediction updating of deteriorating RC structures using inspection information. *Reliab. Eng. Syst. Saf.* **2009**, *94*, 1340–1348. [CrossRef]
35. Bastidas-Arteaga, E.; Chateauneuf, A.; Sánchez-Silva, M.; Bressolette, P.; Schoefs, F. A comprehensive probabilistic model of chloride ingress in unsaturated concrete. *Eng. Struct.* **2011**, *33*, 720–730. [CrossRef]
36. Lizarazo-Marriaga, J.; Higuera, C.; Guzmán, I.; Fonseca, L. Probabilistic modelling to predict fly-ash concrete corrosion initiation. *J. Build. Eng.* **2020**, *30*, 101296. [CrossRef]
37. Zhang, Y.; Zhang, M.; Ye, G. Influence of moisture condition on chloride diffusion in partially saturated ordinary Portland cement mortar. *Mater. Struct.* **2018**, *51*, 36. [CrossRef]
38. Imounga, H.M.; Bastidas-Arteaga, E.; Pitti, R.M.; Ango, S.E.; Wang, X.H. Bayesian assessment of the effects of cyclic loads on the chloride ingress process into reinforced concrete. *Appl. Sci.* **2020**, *10*, 2040. [CrossRef]
39. Zacchei, E.; Nogueira, G.C. Calibration of boundary conditions correlated to the diffusivity of chloride ions: An accurate study for random diffusivity. *Cem. Concr. Compos.* **2022**, *2022*, 104346. [CrossRef]
40. Bentz, D.P.; Guthrie, W.S.; Jones, S.Z.; Martys, N.S. Predicting service life of steel reinforced concrete exposed to chlorides. *Concr. Int.* **2014**, *36*, 55–64.
41. Kim, Y.Y.; Lee, B.-J.; Kwon, S.-J. Evaluation Technique of Chloride Penetration Using Apparent Diffusion Coefficient and Neural Network Algorithm. *Adv. Mater. Sci. Eng.* **2014**, *2014*, 647243. [CrossRef]
42. Fu, C.; Jin, X.; Ye, H.; Jin, N. Theoretical and Experimental Investigation of Loading Effects on Chloride Diffusion in Saturated Concrete. *J. Adv. Concr. Technol.* **2015**, *13*, 30–43. [CrossRef]
43. Zacchei, E.; Nogueira, C.G. 2D/3D Numerical Analyses of Corrosion Initiation in RC Structures Accounting Fluctuations of Chloride Ions by External Actions. *KSCE J. Civ. Eng.* **2021**, *25*, 2105–2120. [CrossRef]
44. Fu, C.; Jin, X.; Jin, N. Modeling of chloride ions diffusion in cracked concrete. In *Earth and Space 2010: Engineering, Science, Construction, and Operations in Challenging Environments*; ASCE: Honolulu, HI, USA, 2010; pp. 3579–3589.
45. Kong, J.S.; Ababneh, A.; Frangopol, D.; Xi, Y. Reliability analysis of chloride penetration in saturated concrete. *Probabilistic Eng. Mech.* **2002**, *17*, 305–315. [CrossRef]

46. Bažant, Z.P.; Najjar, L.J. Nonlinear water diffusion in nonsaturated concrete. *Mater. Struct.* **1972**, *5*, 3–20. [CrossRef]
47. Fan, W.J.; Wang, X.Y. Prediction of Chloride Penetration into Hardening Concrete. *Hind. Publis. Corp.* **2015**, *2015*, 616980. [CrossRef]
48. Halamickova, P.; Detwiler, R.J.; Bentz, D.; Garboczi, E.J. Water permeability and chloride ion diffusion in portland cement mortars: Relationship to sand content and critical pore diameter. *Cem. Concr. Res.* **1995**, *25*, 790–802. [CrossRef]
49. Chen, W.; Zhang, J.; Zhang, J. A variable-order time-fractional derivative model for chloride ions sub-diffusion in concrete structures. *Fract. Calc. Appl. Anal.* **2013**, *16*, 76–92. [CrossRef]
50. Fish, J.; Belytschko, T. *A First Course in Finite Elements*; John Wiley & Sons, Ltd.: Hoboken, NJ, USA, 2007; 344p.
51. Dattoli, G. Generalized polynomials, operational identities and their applications. *J. Comput. Appl. Math.* **2000**, *118*, 111–123. [CrossRef]
52. Dattoli, G.; Torre, A.; Carpanese, M. Operational rules and arbitrary order Hermite generating functions. *J. Math. Anal. Appl.* **1998**, *227*, 98–111. [CrossRef]
53. Yari, A.; Mirnia, M. Direct method for solution variational problems by using Hermite polynomials. *Bol. Soc. Paran. Mat.* **2021**, *39*, 223–237. [CrossRef]
54. ACI 117-10; Specification for Tolerances for Concrete Construction and Materials (ACI 117-10) and Commentary (ACI 117R-10). American Concrete Institute (ACI): Farmington Hills, MI, USA, 2010. Available online: https://www.dli.pa.gov/ucc/Documents/2018-ICC-Code-Review-Public-Comments/Szoke-117-10.pdf (accessed on 9 July 2021).
55. Andrade, C.; Diez, J.M.; Alonso, C. Mathematical modelling of a concrete surface "skin effect" on diffusion in chloride contaminated media. *Adv. Cem. Based Mater.* **1997**, *6*, 39–44. [CrossRef]
56. Kreijger, P.C. The skin of concrete composition and properties. *Matériaux Et Constr.* **1984**, *17*, 275–283. [CrossRef]
57. Morga, M.; Marano, G.C. Chloride penetration in circular concrete columns. *Int. J. Concr. Struct. Mater.* **2015**, *9*, 173–183. [CrossRef]
58. Camara, A.; Kavrakov, I.; Nguyen, K.; Morgenthal, G. Complete framework of wind-vehicle-bridge interaction with random road surfaces. *J. Sound Vib.* **2019**, *458*, 197–217. [CrossRef]
59. Apostolopoulos, C.A.; Papadakis, V.G. Consequences of steel corrosion on the ductility properties of reinforcement bar. *Constr. Build. Mater.* **2008**, *22*, 2316–2324. [CrossRef]
60. El Hassan, J.; Bressolette, P.; Chateauneuf, A.; El Tawil, K. Reliability-based assessment of the effect of climatic conditions on the corrosion of RC structures subject to chloride ingress. *Eng. Struct.* **2010**, *32*, 3279–3287. [CrossRef]
61. Bastidas-Arteaga, E.; Bressolette, P.; Chateauneuf, A.; Sánchez-Silva, M. Probabilistic lifetime assessment of RC structures under coupled corrosion-fatigue deterioration processes. *Struct. Saf.* **2009**, *31*, 84–96. [CrossRef]
62. Rodriguez, R.G.; Aperador, W.; Delgado, A. Calculation of chloride penetration profile in concrete structures. *Int. J. Electrochem. Sci.* **2013**, *8*, 5022–5035.
63. Oliveira, H.L.; Chateauneuf, A.; Leonel, E.D. Probabilistic mechanical modelling of concrete creep based on the boundary element method. *Adv. Struct. Eng.* **2018**, *22*, 337–348. [CrossRef]
64. *Wolfram Mathematica 12, Software Version Number 12.0*; Software for Technical Computation; Wolfram Research: Champaign, IL, USA, 2019.